Near-field resonance at far-field induced transparency in diffractive arrays of plasmonic nanorods

S.R.K. Rodriguez,[1,*] O.T.A. Janssen,[2] G. Lozano[1], A. Omari[3,4], Z. Hens[3,4], and J. Gómez Rivas[1,5]

[1] *Center for Nanophotonics, FOM Institute AMOLF, c/o Philips Research Laboratories High Tech Campus 4, 5656 AE Eindhoven, The Netherlands*

[2] *Optics Research Group, Delft University of Technology, 2628 CJ Delft, The Netherlands*

[3] *Center for Nano and Biophotonics, Ghent University, Belgium*

[4] *Physics and Chemistry of Nanostructures, Ghent University, Belgium*

[5] *COBRA Research Institute, Eindhoven University of Technology, P.O. Box 513, 5600 MB Eindhoven, The Netherlands*

[*] *Corresponding author: s.rodriguez@amolf.nl*

Compiled March 6, 2013

We numerically demonstrate that a periodic array of metallic nanorods sustains a maximum near-field enhancement and a far-field induced transparency at the same energy and in-plane momentum. The coupling of bright and dark plasmonic lattice resonances, and electromagnetic retardation along the nanorod length, are responsible for this effect. A standing wave with a quadrupolar field distribution is formed, giving rise to a collective suppression of far-field scattering and simultaneously enhanced local fields.

OCIS codes: 240.6680, 250.5403, 050.2770, 260.5740

Resonance phenomena are at the heart of nearly any approach towards controlling light. The enhancement of an optical system's response at resonance is normally associated with an increased light extinction. In the presence of surface electromagnetic waves, the resonant condition requires a careful reconsideration, since the spectrum of radiation may be different in the near-field (NF) with respect to the far-field (FF) [1–4]. Thus, a frequency of maximum NF enhancement may not coincide with an extinction maximum. Such differences have a profound significance for the field of metallic nano-optics, where optical antennas are commonly designed to manipulate near-fields, but characterized by their far-field spectra [5].

In this Letter we demonstrate through Finite Difference in Time Domain (FDTD) simulations that a diffractive array of plasmonic nanorods sustains a maximum NF enhancement and a FF induced transparency at the same energy and in-plane momentum. This effect can be regarded as a collective counterpart of Electromagnetically Induced Transparency (EIT) in plasmonic systems [6–8]. Therein, destructive interference between two localized modes induces a narrow transparency window within a broad resonance. One of the two modes, henceforth called bright, couples strongly to radiation and has a broad linewidth. The other mode, henceforth called dark, couples weakly to radiation and has a narrow linewidth. Dark modes have attracted interest for the realization of SPASERS [9], subwavelength guiding of optical radiation [10], enhanced spontaneous emission [11], and sensing [12,13]. In this work the bright and the dark mode are both collective resonances (their quality factors increase with the number of particles in the array [14]) rather than localized. A key point we address is how the NF resonance at the FF induced transparency can be designed by varying the length of the nanorods.

All simulations are done with an in-house developed FDTD model [15]. The computational domain consists of a unit cell with Bloch-Floquet boundary conditions on the sides and perfectly matched layers on the top and bottom, wherein the incident wave propagates downwards. We investigate arrays of gold nanorods in a rectangular lattice with constants $a_x = 600$ nm and $a_y = 300$ nm. The surrounding medium is homogeneous with refractive index $n = 1.46$ (silica). The dielectric function of gold is taken from Palik [16], and fitted with a Drude model. The incident light is polarized along the short axis of the nanorods. The transmittance (reflectance) is calculated by integrating the vertical time-averaged Poynting vector on a plane below (above) the array. For the reflectance, the incident field is subtracted. As an indication of the near-field intensity enhancement (NFIE), we compute $|E|^2/|E_0|^2$, with E the total electric field and E_0 the incident field, at a plane intersecting the nanorods at their mid-height.

Figure 1 shows FF and NF spectra for an array of nanorods with dimensions $250 \times 110 \times 40$ nm^3. The zeroth-order transmittance T_0 in Fig. 1(a), reflectance R_0 in Fig. 1(b), NFIE in Fig. 1(d), and $1 - R_0 - T_0$ in Fig. 1(e), are shown in color as a function of the incident photon energy and the wave vector component parallel to the long axis of the nanorods $\vec{k}_{\parallel} = k_0 \sin(\theta_{in})\hat{x}$, with k_0 the magnitude of the free space wave vector. The $(+1, 0)$ and $(-1, 0)$ Rayleigh anomalies (RAs) - diffraction orders radiating in the plane of the array - are indicated by the solid and dash-dot lines, respectively. Their dispersion is given by $E(k_{\parallel}) = \frac{\hbar c}{n}|k_{\parallel} + mG_x|$, where m is the order of diffraction and $G_x = \frac{2\pi}{a_x}$ is the x-component of the reciprocal lattice vector.

The two dips (peaks) in T_0 (R_0) red-shifted with respect to the RAs and following their dispersion are hybrid photonic-plasmonic Fano resonances [17–20]. These

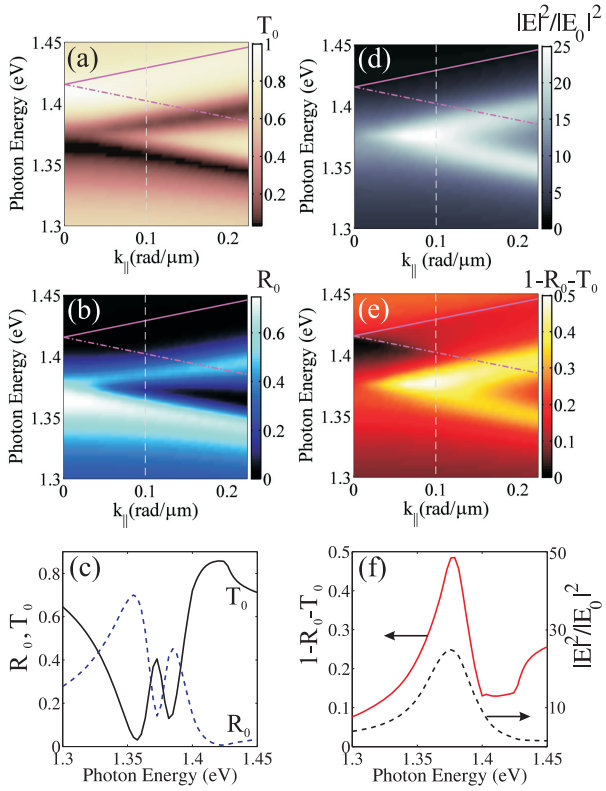

Fig. 1. Zeroth-order (a) Transmittance T_0, (b) Reflectance R_0, and (c) cut of (a) and (b) at $k_{\|} = 0.1$ rad/μm. (d) $1 - R_0 - T_0$, (e) average near field intensity enhancement at a plane intersecting the nanorods at their mid-height, and (f) cut of (d) and (e) as solid red line at $k_{\|} = 0.1$ rad/μm. In (a), (b), (d), and (e), $k_{\|} = 0.1$ rad/μm is indicated by the vertical dashed lines; the solid and dash-dot lines indicate the (+1,0) and (-1,0) Rayleigh anomalies. The nanorods have dimensions $250 \times 110 \times 40$ nm^3. Animations of the real, y-component of the electric field in the plane of the array are shown in Media 1 and Media 2 for the high and low energy extinction peaks in (c). Media 3 holds for the far-field induced transparency between these peaks, which is also at the peak in (f).

are known as Surface Lattice Resonances (SLRs), and their narrow linewidth stems from a collective suppression of radiative damping by the diffractive coupling of localized surface plasmons [14, 21]. The SLR associated with the (-1,0) order is bright, as its dispersion flattens and its extinction increases near normal incidence. In contrast, a narrowing linewidth and diminishing extinction - signatures of subradiant damping - are observed for the (+1,0) SLR as $k_{\|}$ decreases and the mode becomes dark at normal incidence [22]. The mutual coupling of bright and dark SLRs leads to an anti-crossing in their dispersion relation at $k_{\|} = 0$, i.e., a frequency gap opens [22]. This anti-crossing leads to a small gap near 1.37 eV in Figs. 1(a) and Figs. 1(b). Much larger gaps were reported for identical lattices with different

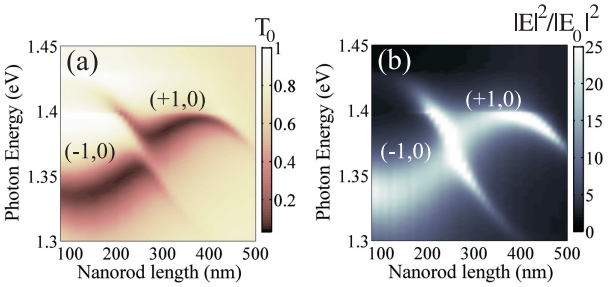

Fig. 2. (a) Zeroth-order Transmittance T_0 and (b) near field intensity enhancement at a plane intersecting the nanorods at their mid-height. Arrays of nanorods with width =110 nm, height = 40 nm, and variable length, are illuminated by a plane wave with $k_{\|} = 0.08$ rad/μm. The labels near the surface lattice resonances indicate the associated diffraction order.

nanorod sizes in Ref. [22].

The NFIE features in Fig. 1(d) are very similar to those observed in R_0 and T_0 in the high $k_{\|}$ regime, but a strong discrepancy arises near $k_{\|} = 0.1$ rad/μm. Figure 1(e) shows $1 - R_0 - T_0$, which for energies below the Rayleigh anomalies is exactly the absorptance in the metal. As expected, there is a close correspondence between absorption and NFIE. In Fig. 1(c) we plot cuts of Fig. 1(a) and Fig. 1(b) at $k_{\|} = 0.1$ rad/μm, and Fig. 1(f) shows cuts of Fig. 1(d) and Fig. 1(e) at the same value of $k_{\|}$, which is indicated by the vertical dashed line in all dispersion diagrams. The dips (peaks) in T_0 (R_0) at 1.355 eV and 1.385 eV in Fig. 1(c) correspond to SLRs associated with the $(-1,0)$ and $(+1,0)$ diffraction orders, respectively. A FF induced transparency is observed as a dip (peak) in R_0 (T_0) between the two SLRs. In contrast, Fig. 1(f) displays a single peak in the NFIE and in absorptance at the same energy of the FF induced transparency.

The contrast between the FF and NF spectrum of this nanorod array derives from the interference between the SLRs, and the associated retardation of the scattered field along the nanorod length. These processes are governed by the geometry of the nanorods, and in particular their length L. Figure 2 shows T_0 in (a) and NFIE in (b), as a function of L, for arrays of nanorods with dimensions $L \times 110 \times 40$ nm^3 illuminated by a plane wave with $k_{||} = 0.08$ rad/μm. The 110 nm width and 40 nm height of these nanorods are identical to those reported in Ref. [22], so direct comparison can be made for $L = 450$ nm. The high and low energy features correspond to the $(+1, 0)$ and $(-1, 0)$ SLRs. Their energy and linewidth vary with L due to retardation and radiative damping. Notice that for $L \gtrsim 250$ nm the (+1,0) SLR is bright, whereas the (-1,0) SLR is dark, as reported in Ref. [22]. The SLR properties are interchanged for $L \lesssim 250$ nm, such that the flattening of the band occurs for the (-1,0) SLR and subradiant damping onsets for the (+1,0) SLR, as observed in Fig 1. Particularly inter-

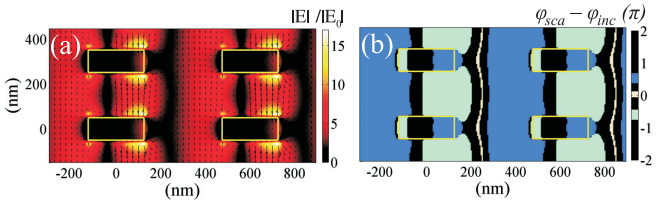

Fig. 3. (a) Field enhancement (in color scale) and real part of the scattered field at an arbitrary phase (arrows), and (b) phase difference between the scattered and incident field in units of π. Both (a) and (b) are calculated at a plane intersecting the nanorods (delimited by the yellow lines) at their mid-height. The incident photon energy and in-plane wave vector correspond to the NF resonance at the FF induced transparency.

esting is the regime 230 nm $\lessapprox L \lessapprox$ 270 nm, where T_0 displays an anti-crossing characteristic of coupled modes, but the NFIE displays a crossing of the two modes. In this regime the structure has a resonant NF at a FF induced transparency, as discussed for Fig. 1.

The field profile at the photon energy and $k_{||}$ of the NF resonance at the FF induced transparency is shown in Fig. 3. Figure 3(a) shows the total electric field enhancement $|E|/|E_0|$ in color and the scattered field as arrows. The four hot-spots near the corners of the nanorods and the scattered field show the quadrupolar character of the mode. The inclined incidence breaks the symmetry of the mode, which manifests as a stronger field enhancement on the right side of each nanorod. This broken symmetry leads to a non-vanishing dipole moment, which allows the excitation of this mode and a finite extinction. Figure 3(b) shows the differences in phase between the scattered and incident fields, i.e., $\phi_{sca} - \phi_{inc}$. Two values, which are $(-0.6 \pm 0.15)\ \pi$ (light blue) and $(0.5 \pm 0.15)\ \pi$ (dark blue), prevail throughout space. Their difference, 1.1π, is close to the out of phase condition of π, thus resulting in a suppression of scattering. The phase distribution in Fig. 3(b) corresponds to the formation of a standing wave. The interference of two counter-propagating surface polaritons (Media 1 and Media 2) creates the standing wave (Media 3, which is the time-evolution of the mode in Fig. 3).

In conclusion, a periodic array of plasmonic nanorods was shown to exhibit a resonant near-field and far-field induced transparency at the same photon energy and in-plane momentum. We envisage this counterintuitive behavior to enable many of the key functionalities (e.g. enhanced light emission and sensing) pursued by plasmonic EIT analogs, but with the benefit of a collective resonance at the expense of tight field localization.

This work was supported by the Netherlands Foundation Fundamental Research on Matter (FOM) and the Netherlands Organization for Scientific Research (NWO), and is part of an industrial partnership program between Philips and FOM. This work is supported byNanoNextNL of the Government of the Netherlands and 130 partners. O.T.A.J. acknowledges the Dutch Technology Foundation STW, which is the applied science division of NWO, and the Technology Programme of the Ministry of Economic Affairs (project number 10301). A.O. acknowledges the Institute for the Promotion of Innovation through Science and Technology in Flanders (IWT-Vlaanderen). Z.H. acknowledges BelSPo (IAP P7/35, photonics@be) and the FWO-Vlaanderen (project nr. G.0794.10) for research funding.

References

1. A. V. Shchegrov, K. Joulain, R. Carminati, and J.-J. Greffet, Phys. Rev. Lett. **85**, 1548 (2000).
2. G. W. Bryant, F. J. Garcia de Abajo, and J. Aizpurua, Nano Lett. **8**, 631 (2008).
3. B. M. Ross and L. P. Lee, Opt. Lett. **34**, 896 (2009).
4. B. Gallinet and O. J. F. Martin, Opt. Express **19**, 22167 (2011).
5. P. Bharadwaj, B. Deutsch, and L. Novotny, Adv. Opt. Photon **1**, 438 (2009).
6. S. Zhang, D. A. Genov, Y. Wang, M. Liu, and X. Zhang, Phys. Rev. Lett. **101**, 047401 (2008).
7. N. Liu, L. Langguth, T. Weiss, J. Kästel, M. Fleischhauer, T. Pfau, and H. Giessen, Nat. Mat. **8**, 758 (2009).
8. P. Tassin, L. Zhang, T. Koschny, E. N. Economou, and C. M. Soukoulis, Phys. Rev. Lett. **102**, 053901 (2009).
9. D. J. Bergman and M. I. Stockman, Phys. Rev. Lett. **90**, 027402 (2003).
10. M. Liu, T.-W. Lee, S. K. Gray, P. Guyot-Sionnest, and M. Pelton, Phys. Rev. Lett. **102**, 107401 (2009).
11. S. Rodriguez, S. Murai, M. Verschuuren, and J. Gómez Rivas, Phys. Rev. Lett. **109**, 166803 (2012).
12. F. Hao, Y. Sonnefraud, P. V. Dorpe, S. A. Maier, N. J. Halas, and P. Nordlander, Nano Lett. **8**, 3983 (2008).
13. F. Neubrech, A. Pucci, T. W. Cornelius, S. Karim, A. Garcia-Etxarri, and J. Aizpurua, Phys. Rev. Lett. **101**, 157403 (2008).
14. S. Rodriguez, M. Schaafsma, A. Berrier, and J. Gómez Rivas, Physica B: Condensed Matter **407**, 4081 (2012).
15. O. Janssen, "Rigorous simulations of emitting and non-emitting nano-optical structures," Ph.D. thesis, (Delft University, 2010).
16. E. Palik, Handbook of optical constants of solids (Academic Press, New York, 1985).
17. S. Zou and G. C. Schatz, J. Chem. Phys. **121**, 12606 (2004).
18. Y. Chu, E. Schonbrun, T. Yang, and K. B. Crozier, Appl. Phys. Lett. **93**, 181108 (2008).
19. V. G. Kravets, F. Schedin, and A. N. Grigorenko, Phys. Rev. Lett. **101**, 087403 (2008).
20. B. Auguié and W. L. Barnes, Phys. Rev. Lett. **101**, 143902 (2008).
21. W. Zhou, Y. Hua, M. D. Huntington, and T. W. Odom, J. Phys. Chem. Lett. **3**, 1381 (2012).
22. S. Rodriguez, A. Abass, B. Maes, O. Janssen, G. Vecchi, and J. Gómez Rivas, Phys. Rev. X **1**, 021019 (2011).

Informational Fourth Page

Full versions of citations.

References

1. A. V. Shchegrov, K. Joulain, R. Carminati, and J.-J. Greffet, "Near-Field Spectral Effects due to Electromagnetic Surface Excitations," Phys. Rev. Lett. **85**, 1548 (2000).
2. G. W. Bryant, F. J. Garcia de Abajo, and J. Aizpurua, "Mapping the Plasmon Resonances of Metallic Nanoantennas," Nano Lett. **8**, 631 (2008).
3. B. M. Ross and L. P. Lee, "Comparison of near- and far-field measures for plasmon resonance of metallic nanoparticles," Opt. Lett. **34**, 896 (2009).
4. B. Gallinet and O. J. F. Martin, "Relation between near–field and far–field properties of plasmonic Fano resonances,", Opt. Express **19**, 22167 (2011).
5. P. Bharadwaj, B. Deutsch, and L. Novotny, "Optical Antennas," Adv. Opt. Photon **1**, 438 (2009).
6. S. Zhang, D. A. Genov, Y. Wang, M. Liu, and X. Zhang, "Plasmon Induced Transparency in Metamaterials," Phys. Rev. Lett. **101**, 047401 (2008).
7. N. Liu, L. Langguth, T. Weiss, J. Kästel, M. Fleischhauer, T. Pfau, and H. Giessen, "Plasmonic analogue of electromagnetically induced transparency at the Drude damping limit," Nat. Mat. **8**, 758 (2009).
8. P. Tassin, L. Zhang, T. Koschny, E. N. Economou, and C. M. Soukoulis, "Low-Loss Metamaterials Based on Classical Electromagnetically Induced Transparency," Phys. Rev. Lett. **102**, 053901 (2009).
9. D. J. Bergman and M. I. Stockman, "Surface Plasmon Amplification by Stimulated Emission of Radiation: Quantum Generation of Coherent Surface Plasmons in Nanosystems," Phys. Rev. Lett. **90**, 027402 (2003).
10. M. Liu, T.-W. Lee, S. K. Gray, P. Guyot-Sionnest, and M. Pelton, "Excitation of Dark Plasmons in Metal Nanoparticles by a Localized Emitter," Phys. Rev. Lett. **102**, 107401 (2009).
11. S. Rodriguez, S. Murai, M. Verschuuren, and J. Gómez Rivas, "Light-emitting waveguide-plasmon polaritons," Phys. Rev. Lett. **109**, 166803 (2012).
12. F. Hao, Y. Sonnefraud, P. V. Dorpe, S. A. Maier, N. J. Halas, and P. Nordlander, "Symmetry Breaking in Plasmonic Nanocavities: Subradiant LSPR Sensing and a Tunable Fano Resonance," Nano Lett. **8**, 3983 (2008).
13. F. Neubrech, A. Pucci, T. W. Cornelius, S. Karim, A. Garcia-Etxarri, and J. Aizpurua, "Resonant Plasmonic and Vibrational Coupling in a Tailored Nanoantenna for Infrared Detection," Phys. Rev. Lett. **101**, 157403 (2008).
14. S. Rodriguez, M. Schaafsma, A. Berrier, and J. Gómez Rivas, "Collective resonances in plasmonic crystals: Size matters," Physica B: Condensed Matter **407**, 4081 (2012).
15. O. Janssen, "Rigorous simulations of emitting and non-emitting nano-optical structures," Ph.D. thesis, (Delft University, 2010).
16. E. Palik, Handbook of optical constants of solids (Academic Press, New York, 1985).
17. S. Zou and G. C. Schatz, "Narrow plasmonic/photonic extinction and scattering line shapes for one and two dimensional silver nanoparticle arrays," J. Chem. Phys. **121**, 12606 (2004).
18. Y. Chu, E. Schonbrun, T. Yang, and K. B. Crozier, "Experimental observation of narrow surface plasmon resonances in gold nanoparticle arrays," Appl. Phys. Lett. **93**, 181108 (2008).
19. V. G. Kravets, F. Schedin, and A. N. Grigorenko, "Extremely Narrow Plasmon Resonances Based on Diffraction Coupling of Localized Plasmons in Arrays of Metallic Nanoparticles," Phys. Rev. Lett. **101**, 087403 (2008).
20. B. Auguié and W. L. Barnes, "Collective Resonances in Gold Nanoparticle Arrays," Phys. Rev. Lett. **101**, 143902 (2008).
21. W. Zhou, Y. Hua, M. D. Huntington, and T. W. Odom, "Delocalized Lattice Plasmon Resonances Show Dispersive Quality Factors," J. Phys. Chem. Lett. **3**, 1381 (2012).
22. S. Rodriguez, A. Abass, B. Maes, O. Janssen, G. Vecchi, and J. Gómez Rivas, "Coupling Bright and Dark Plasmonic Lattice Resonances," Phys. Rev. X **1**, 021019 (2011).

Plasmonics for solid-state lighting: Enhanced excitation and directional emission of highly efficient light sources

Gabriel Lozano[1,*], Davy J. Louwers[2], Said R. K. Rodríguez[1], Shunsuke Murai[1,3], Olaf T. A. Jansen,[2] Marc A. Verschuuren[2] and Jaime Gómez Rivas[1,4,*]

[1]Center for Nanophotonics, FOM Institute AMOLF, c/o Philips Research Laboratories, Eindhoven, The Netherlands
[2]Philips Research Laboratories, Eindhoven, The Netherlands
[3]Department of Material Chemistry, Graduate School of Engineering, Kyoto University, Kyoto, Japan
[4]COBRA Research Institute, Eindhoven University of Technology, Eindhoven, The Netherlands

*To whom correspondence should be addressed: Dr. G. Lozano, Email: lozano@amolf.nl and Prof. J. Gómez-Rivas, email: rivas@amolf.nl, High Tech Campus 4, 5656 AE, Eindhoven, The Netherlands, Tel: +31(0) 402742349, Fax: +31(0) 402746505

SUPPLEMENTARY INFORMATION

In Fig. S1a we present the variable angle extinction spectra of the periodic array of aluminum nanoparticles as a function of the incident angle for s-polarized light. The color curves indicate the onset of diffraction, the so-called Rayleigh anomalies (RAs), of beams diffracted by the array of aluminum particles. The RAs correspond to the condition at which diffracted orders are grazing to the surface of the array. These RAs are calculated taking 1.47, 1.52 or 1.55 as the refractive index of the diffraction medium. The narrow bands of high extinction follow the dispersion of the RAs. The origin of these resonances, known as surface lattice resonances (SLRs), resides in the diffractive coupling of localized surface plasmon polaritons supported by the individual particles. Figure S1b displays the PLDE dispersion diagram for s-polarized emission. The bands of high photoluminescence directional enhancement (PLDE) correspond to SLRs supported by the array observed in extinction.

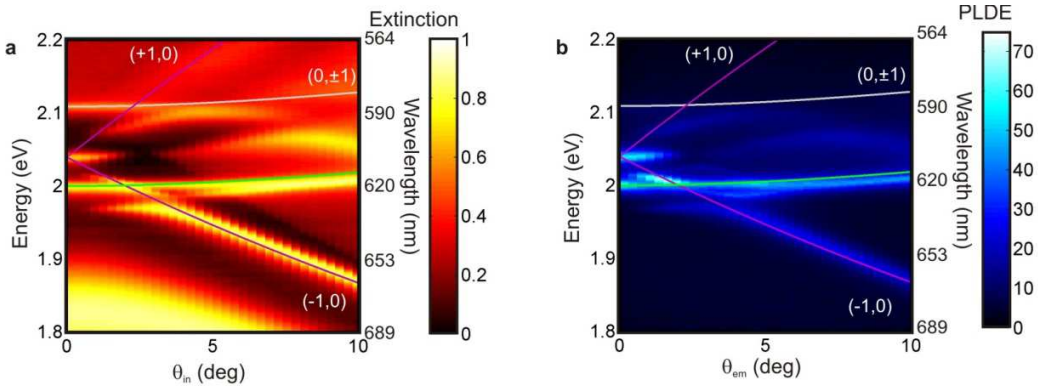

Fig. S1. **a** Extinction of s-polarized light as a function of the photon energy and the angle of incidence θ_{in} of a layer of dye deposited on top of an array of aluminum antennas. **b** s-polarized PLDE as a function of the photon energy and the emission angle θ_{em} measured from the same structure excited with a 2.76 eV

continuous wave laser at θ_{ex}=0 deg. Grey, purple and green curves correspond to the Raleigh anomalies calculated for the beams diffracted in a medium with refractive index 1.47, 1.52 and 1.55, respectively.

Figs. S2, S3, S4 and S5 show FDTD simulations in a plasmonic array of particles covered by a polymer layer. Fig. S2a shows the comparison between measured (black curve) and simulated extinction (grey curve) at θ_{in}=0 deg. The extinction spectra displayed in Fig. S2a show four distinct resonances with different line-widths. On the one hand, one broad resonance is observed at 1.85 eV. On the other, three narrow peaks located at 2.00 eV, 2.04 eV and 2.11 eV stand out. In order to shed light in the origin and field distribution of these resonances, we have performed FDTD simulations on the spatial distribution of the electric field intensity enhancement, i.e. near field intensity normalized by the incident intensity. Results are shown in Figs. S2b-e. Fig. S2b shows the field profile for the broad resonance displayed at 1.85 eV. A high intensity enhancement close to the particles is observed, confirming that this resonance is associated to the excitation of a localized plasmon resonance in the nanoparticles. In contrast, for 2 eV, 2.04 eV and 2.11 eV the field enhancements extend over a large volume around the particles as it is shown in Fig. S2c, S2d and S2e, respectively. These three narrow peaks are associated to the excitation of quasi-bonded surface modes on collective modes supported by the array of aluminum particles. These modes result from the diffractive coupling of localized surface plasmon polaritons. By comparing the different field profiles, it is possible to conclude that the different refractive index layers surrounding the array and the finite thickness of the polystyrene layer have a large impact on the field enhancement distribution. In particular, for 2.11 eV the field extends more into the lower medium, i.e., substrate, than for 2.04 eV and 2.00 eV, leading to a lower effective refractive index for this mode and therefore to a shift of the resonance towards higher energies. Figure S3 shows the spatial distribution of the field intensity enhancement on a plane intersecting the antennas at y=D/2 in a unit cell of the array. The cut presented in S2b does not show the highest values of the near field which are observed nearby the corners of the metallic particle as it is displayed in Fig. S3a. However, it is noteworthy to mention that the electric field enhancement calculated in a particular plane and the extinction of the system should not be compared quantitatively. Specifically, extinction is a far-field magnitude representing the amount of light removed from the forwardly transmitted beam whereas the electric field enhancement is a near-field quantity. Figure S4 shows the dipolar character of the localized surface plasmon resonance observed in extinction at normal incidence and 1.85 eV. Simulations of the total electric field enhancement in a plane intersecting the antennas in their middle height (z=h/2) are shown in Fig. S4. It is considered a plane wave with photon energy 1.85 eV illuminating the array at normal incidence. The field is mostly enhanced at the edges of the nanoantennas displaying a dipolar-like radiation pattern. In Fig. S5, the spatial distribution of the intensity enhancement in a plane parallel to the array at z=270 nm, i.e. within the polymer layer, is presented. It should be noted that only for the 2 eV and 2.04 eV modes the field intensity is significantly enhanced, leading to the large PLDE values experimentally observed.

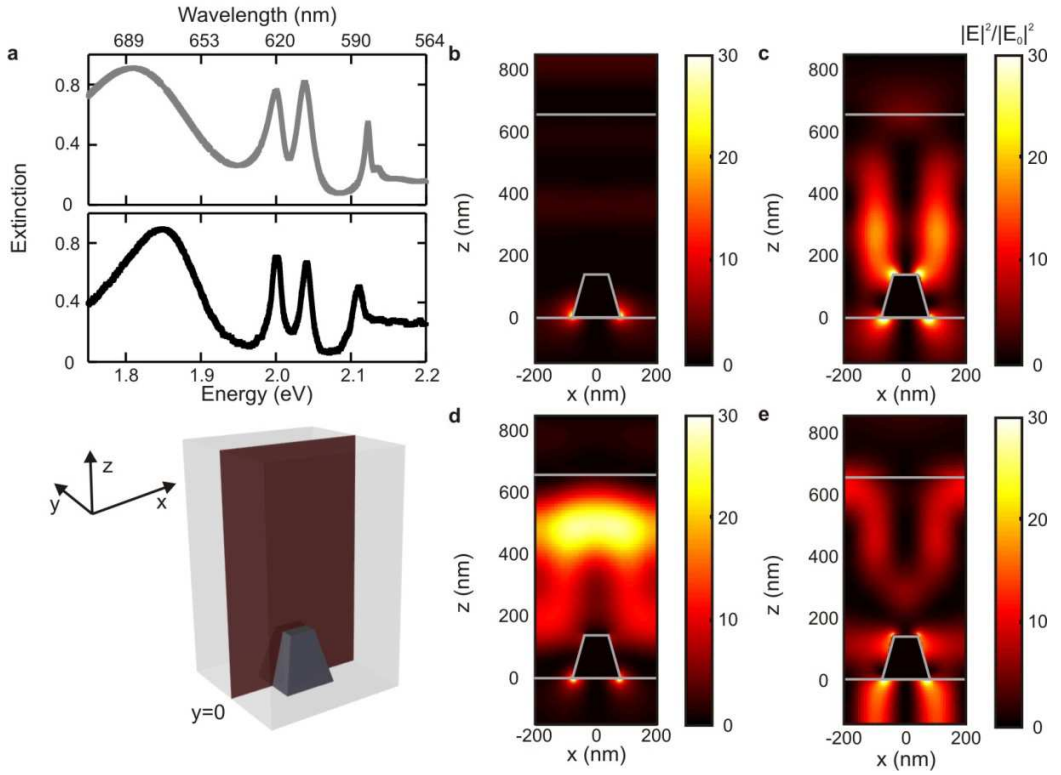

Fig. S2. **a** Measured (black curve, lower panel) and three dimensional FDTD simulated extinction (grey curve, upper panel) spectra at θ_{in}=0 deg of an array of aluminum particles on fused silica covered by a 650 nm thick layer of refractive index 1.59. **b-e** Spatial distribution of the local field intensity enhancement simulated in the same structure. Simulations consider a plane wave incident normal to the array with photon energy **b** 1.85 eV, **c** 2 eV, **d** 2.04 eV and **e** 2.11 eV. The colour plot indicates the intensity enhancement on the plane intersecting the antennas at y=0 in a unit cell of the array. The sketch shows the plane along which the field distributions are calculated. The antenna and the different dielectric interfaces are outlined using grey curves.

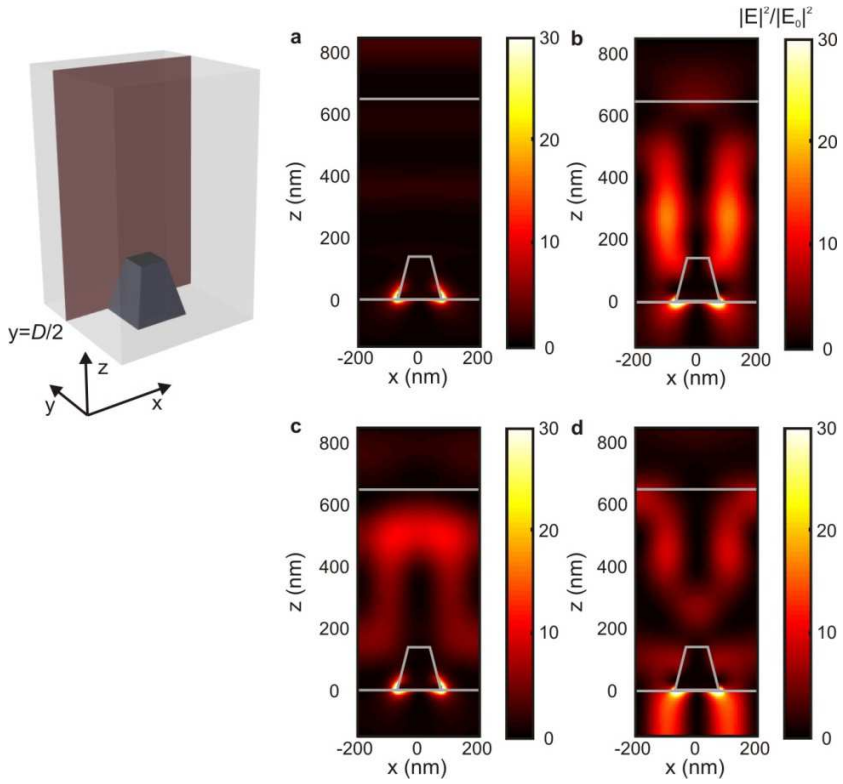

Fig. S3. Spatial distribution of the electric field intensity enhancement simulated in the same structure of Fig S2. Simulations consider a plane wave incident normal to the array with photon energy **a** 1.85 eV, **b** 2 eV, **c** 2.04 eV and **d** 2.11 eV. The colour plot indicates the intensity enhancement on the plane intersecting the antennas at y=*D*/2 in a unit cell of the array. The sketch shows the plane along which the field distributions are calculated. The antenna and the different dielectric interfaces are outlined using grey curves.

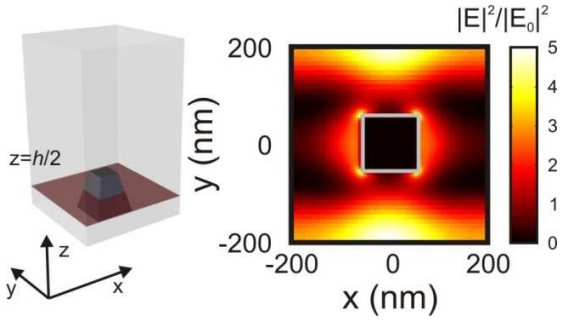

Fig. S4. Spatial distribution of the electric field intensity enhancement simulated in the same structure of Fig. S2. Simulations consider a plane wave incident normal to the array with photon energy 1.85 eV. The colour plot indicates the intensity enhancement on a plane parallel to the array at z=*h*/2 in a unit cell of the array. The sketch shows the plane along which the field distributions is calculated. The antenna is outlined using a grey curve.

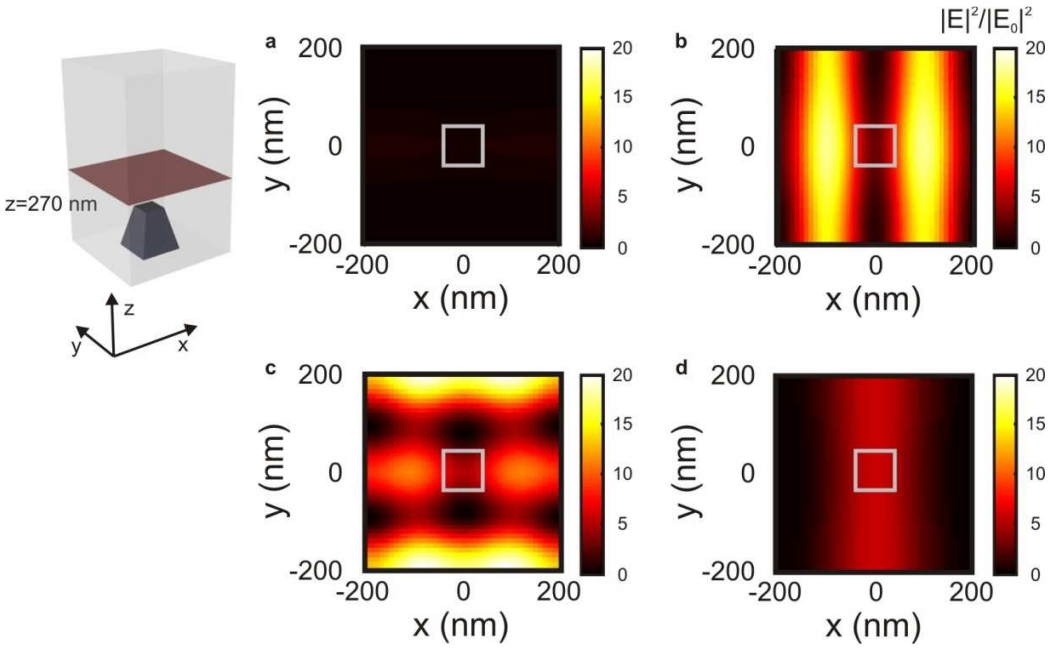

Fig. S5. Spatial distribution of the electric field intensity enhancement simulated in the same structure of Fig. S2. Simulations consider a plane wave incident normal to the array with photon energy **a** 1.85 eV, **b** 2 eV, **c** 2.04 eV and **d** 2.11 eV. The colour plot indicates the intensity enhancement on a plane parallel to the array at z=270 nm in a unit cell of the array. The sketch shows the plane along which the field distributions are calculated. The antenna is outlined using a grey curve.

In Figure S6, we display the PLE spectra as a function of θ_{em} for a broad angular range when the dye molecules are excited at θ_{ex}=0 deg and at θ_{ex}=10 deg. The comparison shows that the dispersive characteristics of the PLDE remain unaltered when θ_{ex} is varied because the directionality in the emission is determined by the resonances at the emission frequencies. However, the overall enhancement is reduced by a factor of two between θ_{ex}=0 and θ_{ex}=10 deg due to the reduction of the pump enhancement. To further illustrate the origin of this difference, in Fig. S7 we present the extinction of the excitation light (2.76 eV) as a function of the incident angle, showing a strong correlation between the amount of blue light transmitted through the sample and the integrated PLDE. At θ_{in}=0 deg the extinction is significantly higher than at θ_{in}=10 deg, indicating that for this frequency and the angle of incidence the nanoparticle array is resonant. This is attributed to the (-1,1) SLR. This resonant behavior leads to the more efficient excitation of the dye and the higher PLE at θ_{ex}=0 deg compared to θ_{ex}=10 deg.

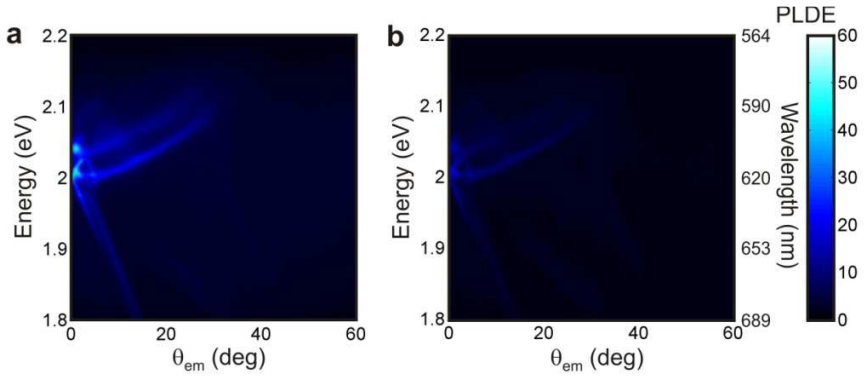

Fig. S6. PLDE as a function of the photon energy and the emission angle, θ_{em}, measured from an emitting layer deposited on top of a plasmonic structure when pumping with a 2.76 eV continuous wave laser at **a** θ_{ex}=0 deg and **b** θ_{ex}=10 deg.

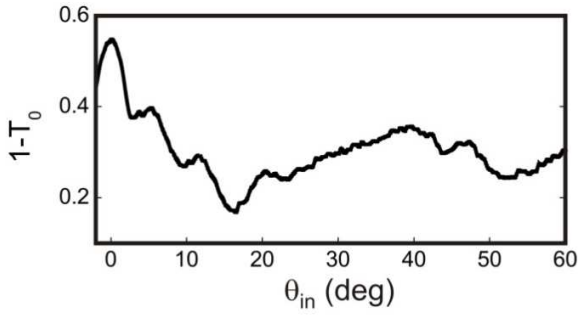

Fig. S7. Extinction spectrum of the periodic array of aluminum nanoantennas measured at 2.76 eV as a function of the angle of incidence, θ_{in}.

To clarify the influence of the periodicity in the plasmonic structure on the PL enhancement, we have deposited a dye layer with the same concentration and the same thickness on top of a random array of similar nanoantennas. A SEM picture of such array is shown as an inset in Fig. S8a. This random array supports localized surface plasmon polaritons but not SLRs. In Figs. S8a-b we show extinction and PLDE measurements as a function of θ_{in} and θ_{em}, respectively. We find a comparable enhancement factor (~3) for the random and the periodic array when measuring the PL far from any SLR, i.e. at θ_{em}=50 deg or at θ_{em}=0 and 1.85 eV. However, this value is much lower than the maximum measured for the periodic array close to the forward direction.

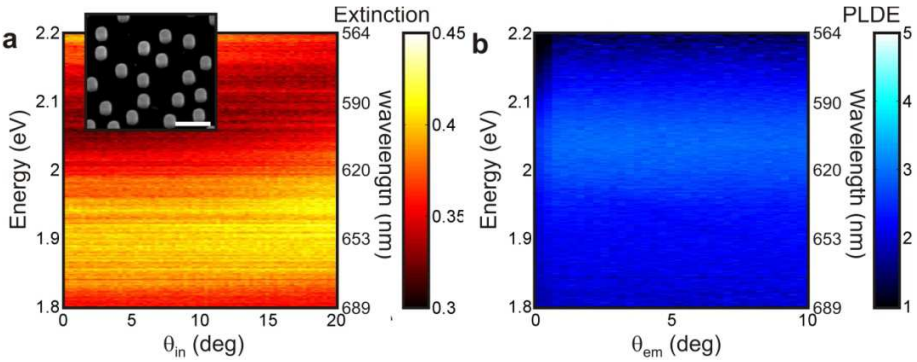

Fig. S8. **a** Extinction of unpolarized light as a function of the photon energy and the angle of incidence, θ_{in}, measured from a layer of light emitters deposited on top of an array of metallic particles randomly arranged. Inset: SEM picture of such random array. Scale bar indicates 500 nm. **b** Unpolarized PLDE as a function of the photon energy and the angle of emission, θ_{em}, measured from the same structure when pumping with a 2.76 eV continous wave laser at θ_{ex}=0 deg.

Prior to the life time measurements of the dye on plasmonic structures, the concentration quenching effect on the decay rate was studied. Figure S9 displays the fitted decay rates as a function of dye concentration in polystyrene. We find significant concentration quenching effects when the fraction of dye in the polymer is above 5 wt%.

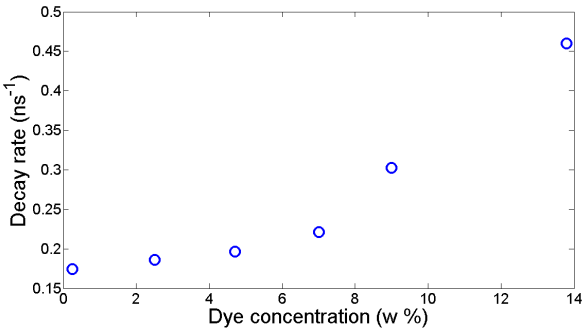

Fig. S9. Total decay rate of excited dye molecules as a function of the weight fraction of dye present in the polymer matrix.

We have also measured variable angle extinction (see Fig. S10a) and emission spectra (see Fig. S10b) from a polymer layer doped with the same die but deposited on top of an array of similar antennas in which the LSPR is blue shifted respect to the measurements shown in Fig. 2a. The spectral position of the LSPR overlaps with the maximum of dye emission for this geometry, leading to a similar PLDE factor. In either case, the improvement associated to localized plasmon resonances is far lower than the one attained from the periodic structure close to the forward direction.

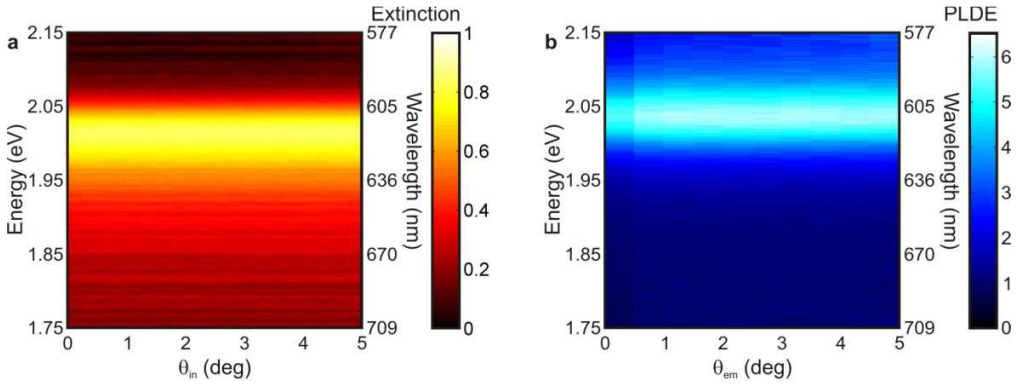

Fig. S10. Extinction of p-polarized light as a function of the photon energy and the angle of incidence θ_{in} of a layer of dye deposited on top of an array of aluminum antennas. **b** p-polarized PLDE as a function of the photon energy and the emission angle θ_{em} measured on the same structure excited with a 450 nm continuous wave laser at θ_{ex}=0 deg.